FLATNESS-BASED CONTROL OF A PARALLEL ROBOT ACTUATED BY PNEUMATIC MUSCLES

Harald Aschemann * and Eberhard P. Hofer *

* *Dept. of Measurement, Control and Microtechnology, University of Ulm, 89081 Ulm, Germany*
e-mail:{harald.aschemann,ep.hofer}@e-technik.uni-ulm.de

Abstract: This paper presents a flatness-based control for a two-degree-of-freedom parallel robot driven by two pairs of pneumatic muscle actuators. The robot consists of a light-weight closed-chain structure with four moving links connected by revolute joints. The two base joints are active and driven by pairs of pneumatic muscles by means of a toothed belt and pulley. Exploiting differential flatness with end-effector position and mean muscle pressures as flat outputs, a cascaded trajectory control is designed. Simulation results demonstrate an excellent control performance and point out the potential of this novel robot.

Keywords: Model-based control, robotics, nonlinearity, mechanisms, pneumatic systems

1. INTRODUCTION

Pneumatic muscles are tension actuators, which consist of a fibre-reinforced vulcanised rubber tubing with connection flanges at both ends. The working principle is based on the specially designed fibre structure that leads to a muscle contraction in longitudinal direction when the pneumatic muscle is filled with compressed air by means of a proportional valve. Pneumatic muscles offer several advantages in comparison to classical cylinders: significantly less weight, no stick-slip effects, insensitivity to dirty working environment, and a larger maximum force. The achievable closed-loop performance using such pneumatic muscle actuators in combination with sophisticated non-linear control has already been investigated thoroughly by experiments at a one-degree-of-freedom test rig (Aschemann and Hofer, 2004). This experimental platform consists of a carriage with pneumatic muscles arranged at opposite sides, which allow for rectilinear movements on two guideways. Current research at the University of Ulm involves the use of pneumatic muscles as actuators for parallel robots, which are known for providing high stiffness, and especially for the capability of performing fast and highly accurate motions of the end-effector.

The parallel robot, which serves as a platform for the development and the investigation of non-linear control approaches, is depicted in fig. 1. It is characterised by a closed-chain kinematic structure formed by four moving links and the robot base offering two degrees of freedom. All joints are revolute joints, two of which - the cranks - are actuated by a pair of pneumatic muscles, respectively. Here, the coordinated contraction of a pair of pneumatic muscles is transformed into a rotation of the according crank by means of a toothed belt and a pulley. The mass flow rate of compressed air into and out of a pneumatic muscle is controlled by means of a proportional valve. The incoming air is available at a maximum pressure of 7 *bar*, whereas the outlet air is discharged at atmospheric pressure, i.e. 1 *bar*. To avoid pressure

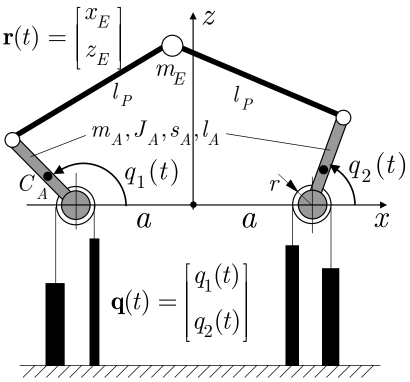

Fig. 1. Two-degree-of-freedom parallel robot driven by pneumatic muscles

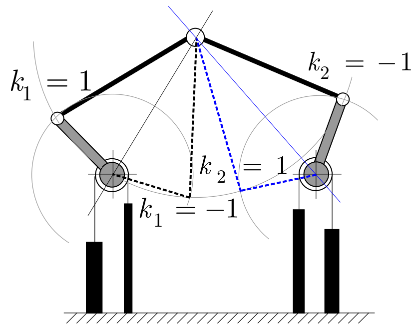

Fig. 2. Ambuigity of the inverse kinematics

declines when large mass flow rates are required, a compensator reservoir for each muscle is utilised.

In this paper, the modelling of the mechatronic system is addressed first. Second, after proving the flatness property for the proposed flat output candidates, a cascade control based on differential flatness is envisaged for the resulting non-linear system model. The control design for the inner control loops involves decentralised pressure controls for each pneumatic muscle with high bandwidth, whereas the central outer control loop design deals with decoupling control of the end-effector position in the xz-plane and the two mean pressures of both pairs of pneumatic muscles. Thus, desired trajectories for the end-effector position in the xz-plane and the two mean pressures of the according pairs of pneumatic muscles can be tracked independently with high accuracy. The trajectory control of the mean pressure represents an effective means for increasing stiffness concerning disturbance forces acting on the end-effector (Bindel *et al.*, 1999). Simulation results of the closed-loop system show excellent tracking performance as well as steady-state accuracy.

2. NON-LINEAR SYSTEM MODELLING

As for modelling, the mechatronic system under consideration is divided in a mechanical system part and a pneumatic system part, which are coupled by the torques resulting from the tension forces of the pair of pneumatic muscles, respectively. Here, as opposed to the model of (Carbonell *et al.*, 2001), the dynamics of the internal muscle pressures is also taken into account.

2.1 Modelling of the Parallel Robot

The chosen multi-body model of the parallel robot part consists of three rigid bodies (fig. 1): the two cranks as actuated links with identical properties (mass m_A, reduced mass moment of inertia w.r.t. the actuated axis J_A, center of gravity distance s_A to the centre of gravity C_A, length of the link l_A, pulley radius r) and the end-effector E (mass m_E), which can be modelled as lumped mass. The inertia properties of the remaining two links with length l_P, which are designed as light-weight construction, shall be neglected in comparison to the other links.

The inertial xz-coordinate system is chosen in the middle of the straight line that connects both base joints with distance $2a$, as depicted in (fig. 1). The motion of the parallel robot is completely described by introducing two generalised coordinates $q_1(t)$ and $q_2(t)$ that denote the two crank angles, which are combined in the vector $\mathbf{q} = [q_1, q_2]^T$. Analogously, the vector of the end-effector coordinates is defined as $\mathbf{r} = [x_E, z_E]^T$.

For a given end-effector position $\mathbf{r}$ the corresponding crank angles follow from the inverse kinematics $\mathbf{q} = \mathbf{q}(\mathbf{r}, k_1, k_2)$, which can be determined in symbolic form. The given ambuigity is taken into account by introducing the configuration parameters k_1 and k_2 as shown in fig. 2. The relationship between the corresponding velocities is obtained by differentiation $\dot{\mathbf{q}} = \mathbf{J}(\mathbf{r}, k_1, k_2)\dot{\mathbf{r}}$, where $\mathbf{J}(\mathbf{r}, k_1, k_2)$ denotes the Jacobian. Analogously, the acceleration relationship is given by $\ddot{\mathbf{q}} = \mathbf{J}(\mathbf{r}, k_1, k_2)\,\ddot{\mathbf{r}} + \dot{\mathbf{J}}(\mathbf{r}, k_1, k_2)\,\dot{\mathbf{r}}$.

The direct kinematics yields the vector of end-effector coordinates for given crank angles, i.e. $\mathbf{r} = \mathbf{r}(\mathbf{q}, k_3)$. Similar to the inverse kinematics, the configuration parameter k_3 is introduced to cope with two possible configurations. The relationships between velocities and between accelerations are derived by taking advantage of the inverse dynamics. This leads directly to $\dot{\mathbf{r}} = \mathbf{J}^{-1}(\mathbf{q}, k_1, k_2, k_3)\dot{\mathbf{q}}$ and $\ddot{\mathbf{r}} = \mathbf{J}^{-1}(\mathbf{q}, k_1, k_2, k_3)[\ddot{\mathbf{q}} - \dot{\mathbf{J}}(\mathbf{q}, k_1, k_2, k_3)\dot{\mathbf{r}}]$. At this, singularities in the Jacobian can be avoided by model-based trajectory planning.

The according equations of motion for the actuated links follow directly from the free-body diagramm applying Euler's Law

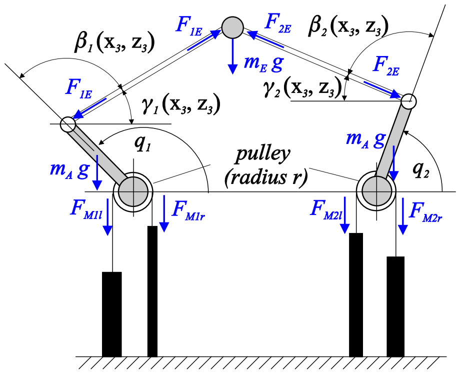

Fig. 3. Free-body diagram of the parallel robot

$$J_A \cdot \ddot{q}_1 = \tau_1 - m_A \cdot g \cdot s_A \cdot \cos q_1 + F_{1E} \cdot l_A \cdot \sin\beta_1 + \eta_1, \tag{1a}$$

$$J_A \cdot \ddot{q}_2 = \tau_2 - m_A \cdot g \cdot s_A \cdot \cos q_2 - F_{2E} \cdot l_A \cdot \sin\beta_2 + \eta_2. \tag{1b}$$

Here, the drive torque τ_i of drive i depends on the corresponding muscle forces, i.e. $\tau_i = r \cdot [F_{Mil} - F_{Mir}]$. The disturbance torque η_i accounts for friction effects as well as remaining uncertainties in the muscle force characteristics (5) of drive i, respectively. The coupling forces F_{1E} and F_{2E} are obtained from Newton's Second Law applied to the end-effector

$$\begin{bmatrix} m_E \cdot \ddot{x}_E \\ m_3 \cdot (g + \ddot{z}_E) \end{bmatrix} = \begin{bmatrix} \cos\gamma_1 & -\cos\gamma_2 \\ \sin\gamma_1 & \sin\gamma_2 \end{bmatrix} \begin{bmatrix} F_{1E} \\ F_{2E} \end{bmatrix} \tag{2}$$

The equations of motion in minimal form for the crank angles can be obtained in two steps. First, the last equation has to be solved for the unknown forces F_{iE}, which then can be eliminated in (1a) and (1b). Second, the substitution of the variables $\gamma_i = \gamma_i(\mathbf{q})$, $\beta_i = \beta(\mathbf{q})$, and $\ddot{\mathbf{r}} = \ddot{\mathbf{r}}(\mathbf{q}, \dot{\mathbf{q}}, \ddot{\mathbf{q}})$ resulting from direct kinematics leads to the envisaged minimal form of the equations of motion

$$\ddot{\mathbf{q}} = \ddot{\mathbf{q}}(\mathbf{q}, \dot{\mathbf{q}}, \tau_1, \tau_2). \tag{3}$$

2.2 Modelling of the Pneumatic Actuators

The parallel robot is equipped with four pneumatic muscle actuators. At this, the indices of all variables describing a particular pneumatic muscle are chosen as follows: the first index $i = 1, 2$ denotes the drive under consideration, described by the generalised coordinate $q_i(t)$, whereas the second index $j = l, r$ stands for the mounting position, i.e. for the left or the right pneumatic muscle. A mass flow $\dot{m}_{Mij}$ into the pneumatic muscle leads to an increase in internal pressure p_{Mij}. In the case of a free movable muscle without external forces, the increased internal pressure results in an enlarged tubing diameter associated with a contraction $\Delta\ell_{Mij,free}$ of the muscle in longitudinal direction due to specially arranged fibres. This contraction effect can be exploited to generate forces. The resulting force F_{Mij} of a pneumatic muscle depends non-linearly on the according internal pressure p_{Mij} as well as the contraction length $\Delta\ell_{Mij}$. The contraction lengths of the pneumatic muscles are related to the generalised coordinates, i.e. the crank angles q_{i0}. The position of the crank angle, where the corresponding right pneumatic muscle is fully contracted, is denoted by q_{i0}. Consequently, by considering the transmission consisting of toothed belt and pulley, the following constraints hold for the contraction lengths of the muscles

$$\Delta\ell_{Mil}(q_i) = r \cdot (q_i - q_{i0}), \tag{4a}$$

$$\Delta\ell_{Mir}(q_i) = \Delta\ell_{M,\max} - r \cdot (q_i - q_{i0}). \tag{4b}$$

Here, $\Delta\ell_{M,\max}$ is the maximum contraction given by 25% of the uncontracted length. The force characteristic $F_{Mij}(p_{Mij}, \Delta\ell_{Mij})$ of the pneumatic muscle yields the resulting static tension force for given internal pressure p_{Mij} as well as given contraction length $\Delta\ell_{Mij}$. This non-linear force characteristic has been identified by static measurements and, then, approximated by the following polynomial description

$$F_{Mij} = \bar{F}_{Mij}(\Delta\ell_{Mij}) \cdot p_{Mij} - f_{Mij}(\Delta\ell_{Mij}) = \sum_{m=0}^{3} \left(a_m \cdot \Delta\ell_{Mij}^m\right) \cdot p_{Mi} - \sum_{n=0}^{4} \left(b_n \cdot \Delta\ell_{Mij}^n\right). \tag{5}$$

The dynamics of the internal muscle pressure follows directly from a mass flow balance in combination with the pressure-density relationship. As the maximum internal muscle pressure is limited by a maximum value of $p_{Mij,max} = 7\ bar$, the ideal gas equation $p_{Mij} = \rho_{Mij} \cdot R \cdot T_{Mij}$ can be utilised as accurate description of the thermodynamic behaviour of the compressed air. Here, the density ρ_{Mij}, the gas constant R, and the thermodynamic temperature T_{Mij} are introduced. For the thermodynamic process a polytropic change of state is employed

$$\frac{p_{Mij}}{\rho_{Mij}^n} = const. \quad \text{or} \quad p_{Mij} = \frac{p_0}{\rho_0^n} \cdot \rho_{Mij}^n, \tag{6}$$

where n denotes the identified polytropic exponent. Thus, the relationship between the time derivative of the pressure and the time derivative of the density results in

$$\dot{p}_{Mij} = n \cdot R \cdot T_{Mij} \cdot \dot{\rho}_{Mij}. \tag{7}$$

The mass flow balance for the pneumatic muscle yields

$$\dot{\rho}_{Mij} \cdot V_{Mij} = \dot{m}_{Mij} - \rho_{Mij} \cdot \dot{V}_{Mij}. \tag{8}$$

The volume characteristic of the pneumatic muscle can be approximated with high accuracy by the following non-linear function of both contraction length and muscle pressure, where the coefficients in this polynomial approximation have been identified by measurements

$$V_{Mij}\left(\Delta\ell_{Mij}, p_{Mij}\right) = \sum_{m=0}^{3} a_m \cdot \Delta\ell_{Mij}^{m} \cdot \sum_{n=0}^{1} b_n \cdot p_{Mij}^{n}. \tag{9}$$

Finally, by inserting (7) and (9) into (8), the pressure dynamics for the muscle i becomes

$$\dot{p}_{Mij} = \frac{n}{V_{Mij} + n \cdot \frac{\partial V_{Mij}}{\partial p_{Mij}} \cdot p_{Mij}} \left[R \cdot T_{Mij} \cdot \dot{m}_{Mij} - \frac{\partial V_{Mij}}{\partial \Delta\ell_{Mij}} \cdot \frac{\partial \Delta\ell_{Mij}}{\partial q_i} \cdot p_{Mij} \cdot \dot{q}_i \right]. \tag{10}$$

3. FLATNESS-BASED FEEDBACK CONTROL DESIGN

3.1 Differential Flatness

Differential flatness is a prerequisite for flatness-based control of non-linear systems, which are usually given in state space representation, i.e. $\dot{\mathbf{x}} = \mathbf{f}\left(\mathbf{x}, \mathbf{u}\right)$. A system is denoted as differentially flat (Fliess *et al.*, 1995) if appropriate flat outputs $\mathbf{y} = \mathbf{y}\left(\mathbf{x}, \mathbf{u}, \dot{\mathbf{u}}, \ldots, \mathbf{u}^{(\ell)}\right)$ exist that

(i) allow for expressing all system states $\mathbf{x}$ and all system inputs $\mathbf{u}$ as a function of these flat outputs $\mathbf{y}$ as well as their time derivatives, i.e. $\mathbf{x} = \mathbf{x}\left(\mathbf{y}, \dot{\mathbf{y}}, \ldots, \mathbf{y}^{(\beta)}\right)$ and $\mathbf{u} = \mathbf{u}\left(\mathbf{y}, \dot{\mathbf{y}}, \ldots, \mathbf{y}^{(\beta+1)}\right)$,

(ii) are differentially independent, i.e. they are not connected by differential equations.

If the first condition is fulfilled, the second condition is equivalent to $dim(\mathbf{u}) = dim(\mathbf{y})$.

3.2 Flatness-Based Pressure Control

The non-linear state equation (10) for the internal muscle pressure p_{Mij} represents the basis for the decentralized pressure control. It can be reformulated as

$$\dot{p}_{Mij} = k_{uij}\left(\Delta\ell_{Mij}, p_{Mij}\right) \cdot \dot{m}_{Mij} - k_{pij}\left(\Delta\ell_{Mij}, \Delta\dot{\ell}_{Mij}, p_{Mij}\right) \cdot p_{Mij}. \tag{11}$$

With the internal muscle pressure as flat output candidate $y_{ijp} = p_{Mij}$, (11) can be solved for the mass flow as control input $u_{ijp} = \dot{m}_{Mij}$ and leads to the inverse model for the pressure control

$$\dot{m}_{Mij} = \frac{1}{k_{uij}\left(\Delta\ell_{Mij}, p_{Mij}\right)} \cdot [\dot{p}_{Mij} + k_{pij}\left(\Delta\ell_{Mij}, \Delta\dot{\ell}_{Mij}, p_{Mij}\right) \cdot p_{Mij}]. \tag{12}$$

Since the internal pressure p_{Mij} as state variable is identical to the flat output and $dim\left(y_{ijp}\right) = dim\left(u_{ijp}\right) = 1$ holds, the differential flatness property is proven. The contraction length $\Delta\ell_{Mij}$ as well as its time derivative $\Delta\dot{\ell}_{Mij}$ can be considered as scheduling parameters in a gain-scheduled adaptation of k_{uij} and k_{pij}.

With the internal pressure as flat output, its first time derivative $\dot{p}_{Mij} = v_{ijp}$ is introduced as new control input. Consequently, the state variable of the corresponding Brunovský form has to be provided by means of measurements, i.e. $z_{ijp} = p_{Mij}$. Each pneumatic muscle is equipped with a pressure transducer mounted at the connection flange that connects the muscle with the toothed belt. The scheduling parameter $\Delta\ell_{Mij}$ results from the measured crank angle q_i, which is obtained by an encoder providing high resolution. Furthermore, the second scheduling parameter $\Delta\dot{\ell}_{Mij}$ is derived from the crank angle q_i by means of real differentiation using a $DT1$-System with the transfer function $G_{DT1}(s) = s/(T_1 \cdot s + 1)$. The error dynamics of each muscle pressure p_{Mij} can be asymptotically stabilised by the following control law

$$v_{ijp} = \dot{p}_{Mijd} + \alpha_{ijp} \cdot (p_{Mijd} - p_{Mij}), \tag{13}$$

where the constant α_{ijp} is determined by pole placement. Here, the desired value $\dot{p}_{Mijd}$ can be obtained either by real differentiation of the corresponding control input u_{ij} in (20) or by model-based calculation using only desired values, i.e. $\dot{p}_{Mijd} = \dot{p}_{Mijd}(\mathbf{r}_d, \dot{\mathbf{r}}_d, \ddot{\mathbf{r}}_d, p_{Mid}, \dot{p}_{Mid})$. The corresponding desired trajectories are obtained from a trajectory planning module that provides synchronous time optimal trajectories according to given kinematic constraints. Defining $e_{pij} = p_{Mijd} - p_{Mij}$ as control error w.r.t. the internal muscle pressure, the corresponding error dynamics is governed by the first order differential equation

$$\dot{e}_{pij} + \alpha_{ijp} \cdot e_{pij} = 0. \tag{14}$$

In each input channel, the non-linear valve characteristic (VC) is compensated by pre-multiplying with its approximated inverse valve characteristic (IVC). This inverse valve characteristic is implemented as look-up-table and depends both on the commanded mass flow and on the measured internal pressure.

3.3 Flatness-Based Decoupling Control

For the outer control loop, the following flat output candidates are chosen: the end-effector position in the xz-plane, i.e. x_E and z_E, and the mean pressure for each pair of muscle, i.e. the mean value $p_{Mi} = (p_{Mil} + p_{Mir})/2$ of the left and the right muscle pressure. The trajectory control of the mean pressure allows for increasing stiffness concerning disturbance forces acting on the carriage (Bindel *et al.*, 1999). As the decentralised pressure controls have been assigned a high bandwidth, these four subsidiary controlled muscle pressures p_{Mij} can be considered as ideal control inputs of the outer control loop. Subsequent differentiation of the first two flat output candidates until one of the control inputs appears leads to

$$\begin{aligned} &y_1 = x_E,\ \dot{y}_1 = \dot{x}_E, \\ &\ddot{y}_1 = \ddot{x}_E\left(x_E, z_E, \dot{x}_E, \dot{z}_E, p_{M1j}, p_{M2j}\right), \end{aligned} \quad (15a)$$

$$\begin{aligned} &y_2 = z_E,\ \dot{y}_2 = \dot{z}_E, \\ &\ddot{y}_2 = \ddot{z}_E\left(x_E, z_E, \dot{x}_E, \dot{z}_E, p_{M1j}, p_{M2j}\right), \end{aligned} \quad (15b)$$

whereas the third and fourth flat output candidates directly depend on the control inputs

$$y_3 = p_{M1} = 0.5 \cdot \left(p_{M1l} + p_{M1r}\right), \quad (16a)$$

$$y_4 = p_{M2} = 0.5 \cdot \left(p_{M2l} + p_{M2r}\right), \quad (16b)$$

The differential flatness can be proven as follows: all system states can be directly expressed by the flat outputs and their time derivatives

$$x_E = y_1,\ \dot{x}_E = \dot{y}_1, z_E = y_2,\ \dot{z}_E = \dot{y}_2. \quad (17)$$

Analogously, the internal muscle pressures as inputs are given by the following function of the flat outputs and a finite number of their time derivatives

$$\mathbf{u} = \begin{bmatrix} p_{M1l}\left(y_1, \dot{y}_1, \ddot{y}_1, y_2, \dot{y}_2, \ddot{y}_2, y_3, y_4\right) \\ p_{M1r}\left(y_1, \dot{y}_1, \ddot{y}_1, y_2, \dot{y}_2, \ddot{y}_2, y_3, y_4\right) \\ p_{M2l}\left(y_1, \dot{y}_1, \ddot{y}_1, y_2, \dot{y}_2, \ddot{y}_2, y_3, y_4\right) \\ p_{M2r}\left(y_1, \dot{y}_1, \ddot{y}_1, y_2, \dot{y}_2, \ddot{y}_2, y_3, y_4\right) \end{bmatrix}. \quad (18)$$

The non-linear state transformation that yields the measured state variables of the corresponding Brunovský form, i.e. the end-effector position and the end-effector velocity in $x-$ and z-direction, is given by the direct kinematics of the parallel robot

$$\mathbf{z}_x = \begin{bmatrix} x_E(\mathbf{q}) \\ \dot{x}_E(\mathbf{q}, \dot{\mathbf{q}}) \end{bmatrix},\ \mathbf{z}_z = \begin{bmatrix} z_E(\mathbf{q}) \\ \dot{z}_E(\mathbf{q}, \dot{\mathbf{q}}) \end{bmatrix}, \quad (19)$$

Here, in contrast to the approach presented in (Aschemann and Hofer, 2004), the end-effector acceleration has not to be determined neither by evaluation of the equation of motion (3) nor by a double real differentiation of the measured position signal. By inserting the new defined inputs $v_1 = \ddot{x}_E$, $v_2 = \ddot{z}_E$, $v_3 = p_{M1}$, and $v_4 = p_{M2}$ as well as the transformed states into (18), the inverse dynamics becomes

$$\mathbf{u} = \mathbf{u}\left(\mathbf{z}_x, \mathbf{z}_z, v_1, v_2, v_3, v_4\right). \quad (20)$$

The error dynamics of the end-effector positions x_E and z_E can be asymptotically stabilized with the control laws

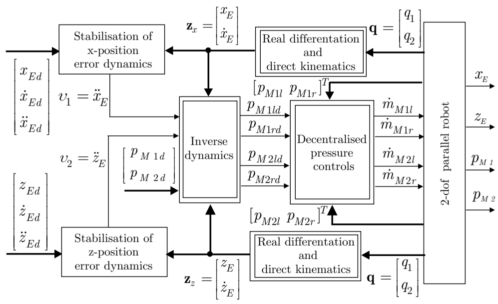

Fig. 4. Control implementation

$$\begin{aligned} v_1 = \ddot{x}_{Ed} &+ \alpha_{2x} \cdot \left(\dot{x}_{Ed} - \dot{x}_E\right) + \alpha_{1x} \cdot \left(x_{Ed} - x_E\right) \\ &+\alpha_{0x} \cdot \int_0^t \left(x_{Ed} - x_E\right) d\tau, \end{aligned} \quad (21a)$$

$$\begin{aligned} v_2 = \ddot{z}_{Ed} &+ \alpha_{2z} \cdot \left(\dot{z}_{Ed} - \dot{z}_E\right) + \alpha_{1z} \cdot \left(z_{Ed} - z_E\right) \\ &+\alpha_{0z} \cdot \int_0^t \left(z_{Ed} - z_E\right) d\tau. \end{aligned} \quad (21b)$$

Here, the desired trajectories for the end-effector position in x-direction x_{Ed} and in z-direction z_{Ed} as well as their first two time derivatives have to be provided, whereas the desired trajectories for the mean pressure of drive 1, i.e. p_{M1d}, and the mean pressure of drive 2, i.e. p_{M2d}, are directly employed in a feedforward manner

$$v_3 = p_{M1d},\quad v_4 = p_{M2d}. \quad (22)$$

Due to the integral control parts, which are meant to counteract the disturbance torque η_i acting on drive i, respectively, and guarantee a vanishing steady-state control error w.r.t. the end-effector position, the dynamics of the corresponding position errors in x-direction $e_x = x_{Ed} - x_E$ as well as in z-direction $e_z = z_{Ed} - z_E$ are of third order. The coefficients α_{2x}, α_{1x}, and α_{0x} as well as α_{2z}, α_{1z}, and α_{0z} are specified by pole placement according to a desired pole configuration. The implementation of the flatness-based control structure is depicted in fig. 4.

4. SIMULATION RESULTS

Tracking performance as well as steady-state accuracy w.r.t. end-effector position and mean pressure have been investigated by simulation studies of a parallel robot with the following dimensions: $a = 0.5\ m$, $l_A = 0.4\ m$, $s_A = 0.2\ m$, $l_P = 0.8\ m$. For this purpose, the tracking of a triangle-like desired trajectory for the controlled variables as shown in fig. 5 has been considered. At this, the desired value for the mean pressure is held constant at 4.0 *bar*.

The first part consists of a motion from the starting point $(x = 0\ m, z = 1\ m)$ to the point $(x = -0.2\ m, z = 0.6\ m)$. The second part comprises a movement in x-direction by

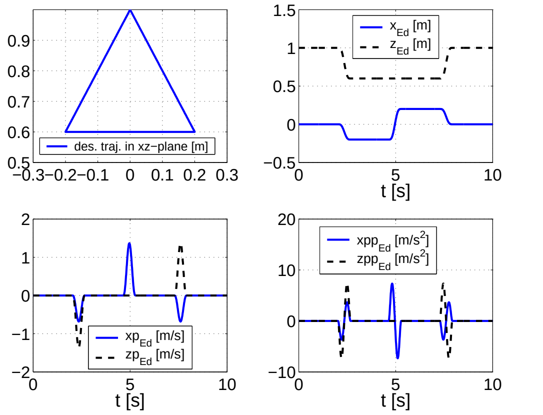

Fig. 5. Desired trajectories and according tracking errors for carriage position and mean pressure

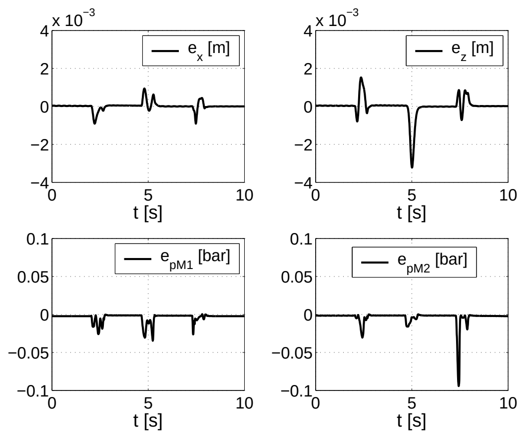

Fig. 6. Tracking errors w.r.t. the end-effector position (top) and the mean pressures (bottom)

0.4 m to the point ($x = 0.2\ m, z = 0.6\ m$). The third part involves the return motion to the starting point. These fast trajectories have been generated considering and, consequently, avoiding saturation effects due to the mass flow limitations.

The corresponding tracking errors are depicted in fig. 6. As for the end-effector position, the maximum tracking errors during the acceleration and deceleration intervals are approx. 3 mm, whereas the steady-state error becomes zero due to the integral control part. Concerning the mean pressure, tracking errors of approx. 0.1 bar occur during the acceleration and deceleration intervals, whereas the steady-state error is less than 0.01 bar.

The corresponding desired values as well as actual values of the decentralised pressure controls are depicted in figure 7. As can be seen, these decentralised control loops achieve an excellent tracking of the desired values provided by the outer decoupling control.

5. CONCLUSIONS

In this paper, a cascaded trajectory control based on differential flatness is presented for a parallel

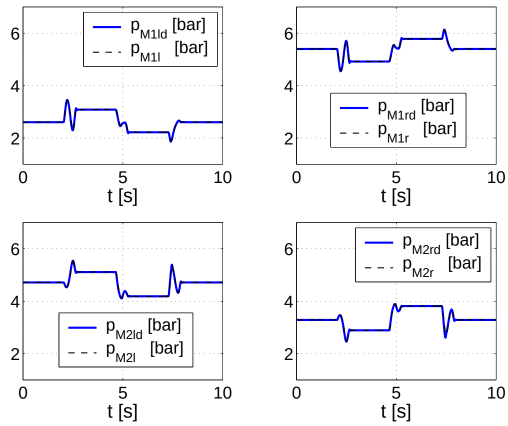

Fig. 7. Desired values and actual values of the four muscle pressures

robot with two degrees of freedom driven by pneumatic muscles. The modelling of this mechatronic system leads to a system of non-linear differential equations of eigth order. For the characteristics of the pneumatic muscles polynomials serve as good approximations. The non-linearity of the valve is linearised by means of a pre-multiplication with its approximated inverse characteristic. The inner control loops of the cascade involve a flatness-based control of the internal muscle pressure with high bandwidth. The outer control loop achieves a decoupling of the end-effector position and the mean pressures as controlled variables. Simulation results emphasise the excellent closed-loop performance with maximum position errors of approx. 3 mm during the movements, vanishing steady-state position error and steady-state pressure error of less than 0.01 bar. Future research will address experiments at a prototype system.

REFERENCES

Aschemann, H. and E.P. Hofer (2004). Flatness-based trajectory control of a pneumatically driven carriage with uncertainties. *Proceedings of NOLCOS 2004, Stuttgart, Germany,* pp. 239–244.

Bindel, R., R. Nitsche, R. Rothfuß and M. Zeitz (1999). Flatness based control of two valve hydraulic joint actuator of a large manipulator. *CD-ROM-Proceedings of ECC 1999, Karlsruhe, Germany.*

Carbonell, P., Z. P. Jiang and D. Repperger (2001). Comparative study of three nonlinear control strategies for a pneumatic muscle actuator. *Proceedings of NOLCOS 2001, Saint-Petersburg, Russia,* pp. 167–172.

Fliess, M., J. Levine, P. Martin and P. Rouchon (1995). Flatness and defect of nonlinear systems: Introductory theory and examples. *Int. J. Control* **61**, pp. 1327–1361.